ELSEVIER

Biophysical Chemistry 127 (2007) 149–154

Biophysical Chemistry

http://www.elsevier.com/locate/biophyschem

Heterogeneous transportation of α_{1B}-adrenoceptor in living cells

Yinghua Guan [a,1], Ming Xu [b,1], Zhangyi Liang [a], Ning Xu [b], Zhizhen Lu [b], Qide Han [b], Youyi Zhang [b,*], Xin Sheng Zhao [a,*]

[a] *Beijing National Laboratory for Molecular Sciences, State Key Laboratory for Structural Chemistry of Unstable and Stable Species, and Department of Chemical Biology, College of Chemistry and Molecular Engineering, Peking University, Beijing 100871, China*

[b] *Institute of Vascular Medicine, Peking University Third Hospital, and Key Laboratory of Molecular Cardiovascular Sciences, Ministry of Education, Peking University, Beijing 100083, China*

Received 27 October 2006; received in revised form 18 January 2007; accepted 21 January 2007
Available online 2 February 2007

Abstract

The heterogeneous motion of α_{1B}-adrenoceptor (α_{1B}-AR) was visualized in living cells with BODIPY-labeled antagonist of AR by single molecule fluorescence microscopy at high spatial resolution. The moving trajectory was reconstructed by precise localization (better than 20 nm) with a least-square fit of a two-dimensional Gaussian point spread function to each single spot. Trajectory analysis revealed two apparent groups of movements: directed motion and hindered motion. The directed motion had speeds higher than 0.1 μm/s. The histogram of diffusion coefficients of the hindered motion showed distinction between the cell membrane and the cytoplasm: the diffusion coefficient was lower near the cell membrane than in the internal cytoplasm, suggesting that α_{1B}-AR was located or trapped in different networks, which was consistent with the natural distribution of cytoskeleton in living cells. These results suggested that the heterogeneity in the motion of α_{1B}-AR in living cell might be associated with different localizations of cell skeleton proteins in the cell, which could provide molecular insight of AR regulation in living cells.

Keywords: Adrenoceptor; Single particle tracking; Living cell

1. Introduction

G protein-coupled receptors (GPCRs), the largest and most diverse family of transmembrane receptors, mediate intracellular responsiveness to numerous extracellular stimuli (such as photons, neurotransmitters, and hormones) [1]. Because of the wide array of cellular processes that are mediated by GPCRs, the study of GPCR regulation holds a prominent position in the field of signal transduction and drug discovery.

Great knowledge has been accumulated on GPCRs by conventional approaches. The signal cascade is triggered when ligands bind to the outside of seven-transmembrane helices, activating the heterotrimeric G protein dissociation [2]. Numerous experiments were employed to investigate the GPCR behaviors, such as dimerization [3–5] and internalization [6,7]. But seldom evidence has ever been established on the dynamic behaviors of GPCRs in a living cell. As a typical member of GPCR family, α_{1B}-adrenoceptor (α_{1B}-AR) plays critical roles in the regulation of a variety of physiological processes such as smooth muscle contraction, myocardial inotropy and chronotropy [8–10]. In living cells, α_{1B}-AR is predominantly located on the cellular surface [6,11,12]. Although extensively studied, some questions are left unknown, such as by which pathway α_{1B}-AR is transferred to the membrane and how it is traveled from the membrane to the internal cytoplasm. These questions are difficult to address by traditional ensemble experiments. For instance, fluorescence recovery after photobleaching (FRAP) [13] can only average over a large number of molecules, and confocal laser scanning

* Corresponding authors. Zhang is to be contacted at Institute of Vascular Medicine, Peking University Third Hospital, and Key Laboratory of Molecular Cardiovascular Sciences, Ministry of Education, Peking University, Beijing 100083, China. Tel./fax: +86 10 82802306. Zhao, Beijing National Laboratory for Molecular Sciences, State Key Laboratory for Structural Chemistry of Unstable and Stable Species, and Department of Chemical Biology, College of Chemistry and Molecular Engineering, Peking University, Beijing 100871, China. Tel.: +86 10 62751727; fax: +86 10 62751708.

E-mail addresses: zhangyy@bjmu.edu.cn (Y. Zhang), zhaoxs@pku.edu.cn (X.S. Zhao).

[1] Contribute equally to this study.

0301-4622/$ - see front matter © 2007 Elsevier B.V. All rights reserved.
doi:10.1016/j.bpc.2007.01.009

microscopy (CLSM) [14,15] is difficult to achieve high time resolution good enough for trajectory tracking.

By removing ensemble averaging, single particle tracking (SPT) [16] and single molecule imaging (SMI) [17] can directly observe the trajectory of individual particle. Thus the spatial and time resolutions can be greatly enhanced, providing information of motion with distinguishable results on different subpopulations. Recently, single virus infection pathway [18,19] in living cells and proceeding model of motor proteins along cytoskeleton [20,21] were reported.

In living cells the receptor movement is not random, but is regulated within a certain time and space. In the present study, with high spatial and fast time resolutions single molecule wide-field fluorescence microscopy was applied to image the accurate transport pathway of constitutive movement of α_{1B}-AR receptor. The dynamic behaviors of α_{1B}-AR in human embryonic kidney (HEK293) living cells were investigated, and the velocities and diffusion coefficients were analyzed. The characteristics of directed motions implied that transport pathways might be alternatively mediated by different cytoskeleton in living cells. The statistics on diffusion coefficients of hindered motion showed obvious distinction between the cell membrane and the cytoplasm, indicating the existence of different network environments in different parts of the cell. This method provided a protocol for imaging fast time-dependent motion trajectory in individual living cell.

2. Materials and methods

2.1. Drugs and plasmid

BODIPY-FL prazosin (excitation/emission 503/512 nm), BODIPY-558/568 prazosin (excitation/emission 558/568 nm) and Tubulin Tracker™ Green reagent (excitation/emission 494/522 nm) were purchased from Molecular Probes. The affinity constant (described as the inhibitory constant pK_i) of BODIPY-labeled prazosin is about 9.0 [22], which is consistent with the affinity constant of prazosin [5,22], a specific antagonist to α_1-AR. The concentration of the fluorescent ligands used in competitive binding was 100 nM, and in wide-field imaging was 10 nm, which are consistent with previous study [11,22]. Phentolamine and nocodazole were purchased from Sigma USA (St. Louis, MO). Bovine serum albumin (BSA) was from Boehringer Mannheim Germany. HEK293 (human embryonic kidney 293) cells and full-length cDNA of human α_{1B}-AR in pDT plasmid were kindly provided by Prof. Kenneth P. Minneman (Emory University, USA).

2.2. Cell culture, transfection, and selection of stably expressed cells

HEK293 cells were maintained in Dulbecco's modified Eagle's medium (DMEM) containing 10% (v/v) fetal bovine serum at 5% CO_2, 37 °C. The cells were transfected with pDT/α_{1B}-AR using Lipofectamine™ 2000 according to the manufacturer's recommendation. α_{1B}-AR stably expressed cells were selected with 800 μg/ml geneticin (G418) and expression level of α_{1B}-AR was determined by radioligand binding assays as described previously [10]. α_{1B}-AR stably expressed HEK293 cells were grown on coverslips for 24 h before use.

2.3. Laser scanning confocal microscopy

α_{1B}-AR stably expressed HEK293 living cells were treated with Tubulin Tracker™ Green reagent according to the manufacturer's recommendation. For the co-localization, after the cells were treated with Tubulin Tracker™ Green reagent for 30 min, cells were incubated with BODIPY-558/568-labeled prazosin for 1 min with the 10 nM concentration and then incubation buffer was washed out and replaced by PBS. The concentration and incubation-time of BODIPY-labeled prazosin were optimized to reach the best resolution of the fluorescence signals. The samples were imaged under a laser scanning confocal microscope (Leica TCS NT, Wetzlar, Germany) using a Plan-Apo 60x oil immersion objective lens. The software used to collect the images was the Leica TCS NT version 1.6.587. The setting on the laser was constant for all experiments. Initial adjustment of the photomultiplier tube (PMT) allowed us to minimize the background while maximizing the fluorescent signals of interest.

2.4. Wide-field imaging microscopy

Before coverslips were mounted on microscope cells were washed three times with phosphate-buffered saline (PBS) at

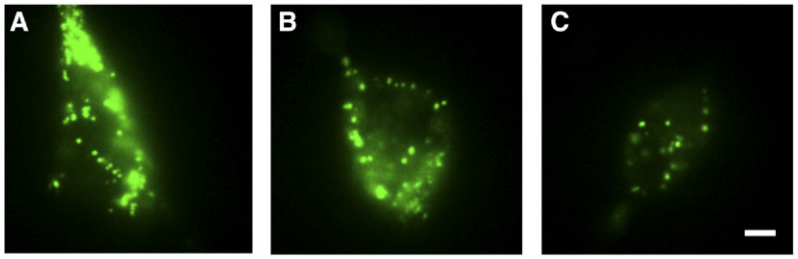

Fig. 1. Inhibition of BODIPY-FL prazosin binding on living α_{1B}-AR HEK293 cells by the competition binding of phentolamine. The α_{1B}-AR stably expressed HEK293 living cells were first treated with BODIPY-FL prazosin (100 nM). Then competition drug phentolamine was added with the final concentrations 0 (A), 10 (B), and 100 (C) μM, respectively. Scale bar is 5 μm.

37 °C. Wide-field fluorescent images were collected several minutes after 10 nM BODIPY-FL prazosin (final concentration) added. At this condition, the best image resolution was obtained. The bath contained 5% BSA with or without the competitive antagonist phentolamine (10 μM, 100 μM) in PBS. A 488 nm (Model 163C, Spectra-Physics) continuous-wave laser beam was introduced into a 100× objective (NA=1.30, oil, Nikon) mounted on an inverted fluorescence microscope (TE300, Nikon, the filters are EX 450–490, DM 505, and BA 520) to excite the cells. The fluorescence emission from molecules was collected by the same objective and imaged onto a charge-coupled device (CCD) camera (Cascade512B, Roper Scientific) with 50 ms exposure time per frame [17].

2.5. Trajectory analysis

Because the physical size of the CCD pixel is 16 μm, with a 100 times objective amplification, the final resolution is 160 nm. This is not enough to get precise positions of the spots. The trajectory of each fluorescence spot was reconstructed in two steps. Firstly, the center pixel of each bright spot in each frame was extracted from the movie stacks. Secondly, a two-dimensional Gaussian point spread function was employed to perform a least-squares fit to each local 7×7 pixels matrix around the center pixel. The collected photons are about 2500 photons, and the photon noise is the main contribution to the uncertainty (about 5 nm) compared with the pixelation and background noise (about 2 nm together). Thus, a precision higher than 10 nm was achieved [23]. The two-dimensional Gaussian point spread function is defined as:

$$P_G = z_0 + A\exp\left[-\frac{1}{2}\left[\left(\frac{(x-x_0)}{s_x}\right)^2+\left(\frac{(y-y_0)}{s_y}\right)^2\right]\right]. \quad (1)$$

Here, the constant term z_0 is contributed by the background fluorescence and detector offset [20], and A is the amplitude. Parameters x_0 and y_0 are the coordinates of the center position, and s_x and s_y are the standard deviations of the distribution in x and y directions, respectively. The diffusion coefficient (D) and directed speed (V) were determined by fitting the plot of a two-dimensional mean-square displacement (MSD) versus time to

$$<\Delta r^2> = 4Dt + (Vt)^2 + C \quad (2)$$

where C is a constant term due to noise [18], and MSD is the average of displacement square of measurement intervals over the whole trajectory:

$$\mathrm{MSD}(t) = <\Delta r^2> = \frac{1}{(N-n)}\sum_{i=1}^{N-n}[(x_{i+1}-x_i)^2 + (y_{i+1}-y_i)^2] \quad (3)$$

where $t=n\Delta t$, N is the total number of frames over the trajectory, and n is the times of frame intervals Δt.

3. Results and discussion

3.1. Specificity of the binding signals in living HEK293 cells

The BODIPY-FL prazosin binding induced fluorescence signals in α_{1B}-AR stably expressed HEK293 living cells is indicated in Fig. 1A, whereas neither BODIPY-FL without prazosin nor living cells without expression of AR could obtain fluorescence images. Furthermore, the fluorescence intensity of BODIPY-FL prazosin (100 nM) treated α_{1B}-AR was reduced by competitive binding with different concentrations (10 μM, 100 μM) of phentolamine, a specific antagonist of α_1-AR (Fig. 1B and C). The fluorescence intensity was much lower in 100 μM phentolamine treated cells than that of 10 μM phentolamine, suggesting that more binding sites of AR were occupied by phentolamine at 100 μM than 10 μM. These results were in agreement with previous studies [22,24,25], pharmacologically showing the specific binding of BODIPY-FL prazosin with α_{1B}-AR in living cells.

3.2. Fluorescence image of tubulin and BODIPY-558/568 prazosin in α_{1B}-AR stably expressed HEK293 living cells

α_{1B}-AR stably expressed HEK293 living cells were pre-incubated with Tubulin Tracker™ Green reagent at the final concentration of 50 nM at 37 °C/5% CO_2. After 30 min, cells were incubated with BODIPY-558/568-labeled prazosin for 1 min (10 nM) and then incubation buffer was washed out and replaced by PBS. Then the fluorescence image of tubulin (excitation/emission 494/522 nm) and fluorescence image of

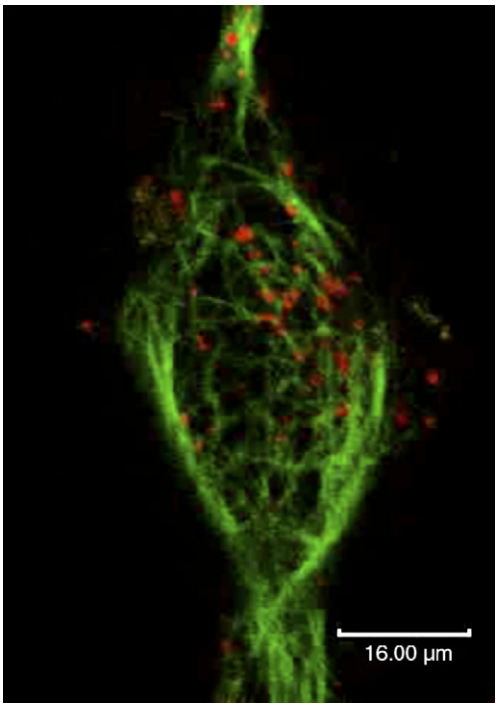

Fig. 2. Confocal scanning fluorescence image of tubulin and BODIPY-558/568 prazosin in an α_{1B}-AR stably expressed HEK293 living cell. The image shows co-localization of fluorescence signals of tubulin and BODIPY-558/568 prazosin (10 nM). Scale bar is 16 μm.

BODIPY-558/568-Praz (excitation/emission 558/568 nm) were collected and merged. The fluorescence image (Fig. 2) shows co-localization of fluorescence signals of tubulin and BODIPY-558/568 prazosin within the resolution limited by optical diffraction, suggesting that the endocytosis pathway of AR might be associated with microtubules in HEK293 living cells. After nocodazole, a microtubule de-polymerizing agent, was added neither the microtubule could be labeled nor the BODIPY-558/568 prazosin could be detected inside the cell.

3.3. Heterogeneity of the motion of α1B-AR in living cells

A wide-field fluorescence image of the BODIPY-prazosin α_{1B}-AR complex is shown in Fig. 3A (up-right inset). The low background fluorescence in the medium buffer or parent cells indicates that the fluorescence from the unbound ligand is negligibly weak. The detected fluorescence signal rooted in the ligand–receptor complex is proportional to the ligand bound to the receptor which is in equilibrium with free ligand. After the center positions were fitted by two-dimensional Gaussian point spread function, the trajectory of each fluorescence spot was reconstructed. Typical trajectories are plotted as black lines in Fig. 3A with red arrows indicating the direction of motion. Heterogeneity of the motion was found not only among particles but also within individual trajectories, which could not be observed by FRAP and CLSM. Two apparent patterns of movements were extracted from the trajectory analysis: restricted motion and directed motion.

The unidirectional translocation exhibits three directions: parallel to the cell surface, from the plasma membrane into the cell and vice versa. Fig. 3B shows the heterogeneity of speed within one trajectory and among different trajectories, with the directed speeds variation from tens to thousands nanometers per second. Stationary and mobile walks can be alternatively found in one trajectory, indicating that the motor proteins could be active or inactive depending on the local environment and viscoelastic properties.

The hindered movement can be found both near the cell periphery and inside the cell (trajectories #1 and #2 in Fig. 3A, B, and further expanded in Fig. 3C). Trajectory #1 represents hindered diffusion near the cell membrane, where the particles were trapped within a small region (about 100 nm) without long distance transportation. As illustrated by trajectory #2 the intracellular trapped diffusion is more mobile comparing to that near the cell membrane.

3.4. Trajectory analysis

After the center positions were determined, the mean-square displacements were calculated. Diffusion coefficients (D) and directed speeds (V) were produced by fitting the plot of MSD versus time (inset of Fig. 4). Histogram of D is shown in Fig. 4A. Most of the diffusion coefficients are less than 0.01 $\mu m^2/s$. After α_{1B}-ARs are synthesized, they are sorted into membranous particles and then transported to the cell surface. On the contrary, during the constitutive motion, receptors may move from the outer surface of the cell into some compartments, and subsequently recycle back to the plasmic membrane. Normally, the compartments or particles have the size of about 50–100 nm in diameter. A spherical particle with diameter of 50–100 nm would have a free diffusion coefficient of 0.23–0.45 $\mu m^2/s$, according to $D=kT/6\pi\eta r$, where η is the cytoplasmic viscosity about 0.01 kg m^{-1} s^{-1}. This means that, in the time interval of 50 ms, the particle has the free

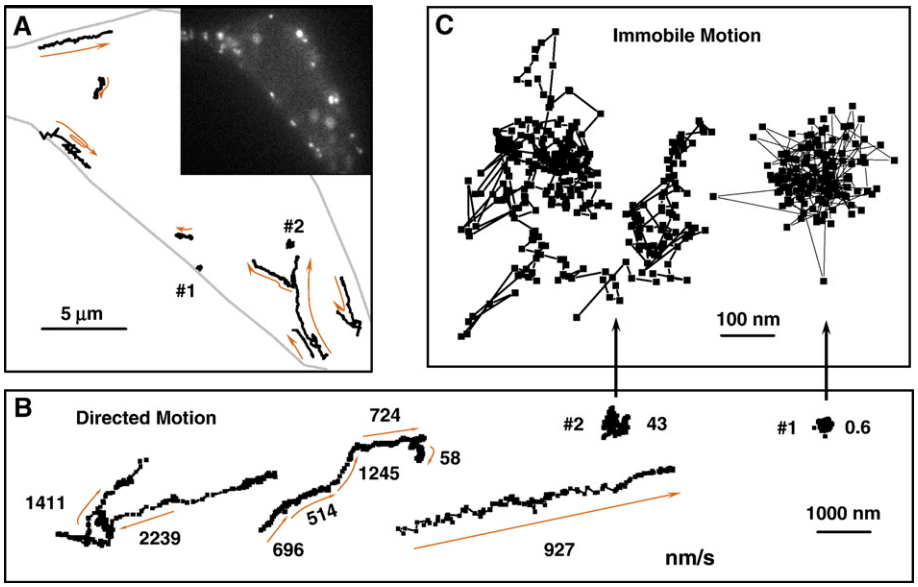

Fig. 3. Heterogeneity of the motion of α_{1B}-adrenoceptor in living cells. (A) A wide-field fluorescence image of a cell (up-right inset) with BODIPY-FL prazosin and some trajectories. The profile of the cell is depicted in gray line and the directions of trajectories are indicated. The scale bar is 5 μm. (B) Five trajectories including three directed and two hindered trajectories. Two of the three directed trajectories are taken from (A), and the other one comes from another cell. The local direction and speed (in nm/s) are indicated in the directed motion. Trajectories #1 and #2 represent the hindered motion near the plasma membrane and in the cytosol, respectively. The scale bar is 1000 nm. (C) The hindered motion is enlarged ten times. Trajectory #2 has more mobile range in each dimension than trajectory #1.

motion range of 0.2–0.3 μm. In our results, the diffusion coefficients are much less than the above-mentioned value, indicating that essentially there is no free diffusion of the spots inside the cell.

The directed speed V has a broad distribution (Fig. 4B). Besides the peak near zero, the distribution showed two distinct populations. One is around 0.2 μm/s and the other is between 0.8 μm/s and 1.0 μm/s. The internal order of eukaryotic cells is established by protein motors transporting molecules and organelles along cytoskeletal filaments [26]. The long distance transportation might be associated with microtubule, because the treatment of the nocodazole can diminish the directed motion (see the movies in the supporting materials). The motion speeds of myosin-V, dynein and kinesin *in vivo* are 0.2, 1.1 and 1.8 μm/s, respectively [27]. The intracellular α_{1B}-ARs could be transported by myosin with low speed or by dynein and kinesin with high speed during the constitutive motion. The intracellular α_{1B}-ARs may be the candidates for its recycling as a reserve receptor pool. Because of the predominant location of α_{1B}-ARs on the cell peripheral region and the extracellular addition of ligands, the motion from out surface to insides was mainly observed, whereas the endogenous receptor moving to the surface was seldom captured.

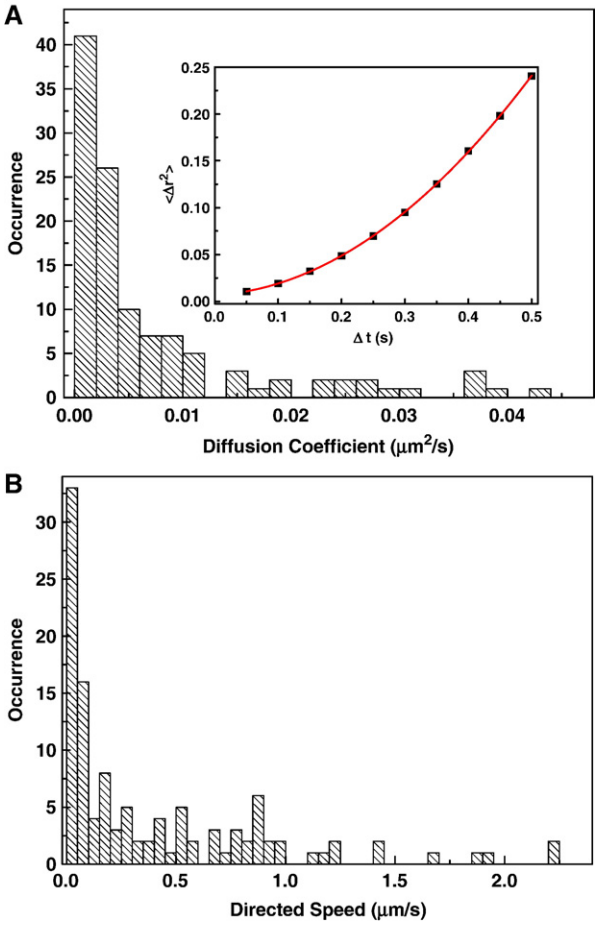

Fig. 4. Statistic analysis of single trajectory. Histogram of the receptor–ligand complex diffusion coefficients (A) and directed speeds (B). (Inset) An example of the plot on measured average mean square displacement $<\Delta r^2>$ versus time (Δt). The line is a fit to $<\Delta r^2>=4D\Delta t+(V\Delta t)^2+C$ with $D=0.0096$ μm²/s, $V=0.93$ μm/s, and the constant $C=0.006$ μm²/s. The constant term is due to noise. The directed motions possess such superlinear shape, whereas the free motions have a linear relationship.

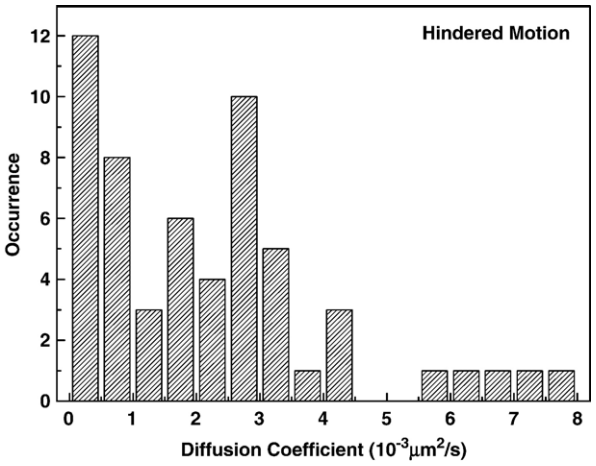

Fig. 5. Histogram of diffusion coefficients of the hindered motion. Diffusion coefficients were derived from the fit (see details in text). Most of the diffusion coefficients near 0.00025 μm²/s come from the trajectories near the plasma membrane, whereas the trajectories in the cytosol contribute to the distribution near 0.00275 μm²/s, indicating that the receptor–ligand complex has less mobile range near the plasma membrane than in the cytosol.

3.5. Diffusion coefficients of the restricted motion near the plasma membrane and inside the cytosol

The distribution of diffusion coefficients of the restricted motion is shown in Fig. 5. This distribution shows more detailed information than an average value obtained by FRAP. There are two main peak values around 0.00025 and 0.00275 μm²/s, respectively. Most of the diffusion coefficients less than 0.001 μm²/s came from the cell peripheral region (for example #1 in Fig. 3A). The particles in the cytosol (for example #2 in Fig. 3A) contributed to the diffusion coefficients around 0.00275 μm²/s. The diffusion is random migration of small particles arising from thermal energy. The more viscous the environment is, the smaller the diffusion coefficient will be. The fact that the diffusion coefficient is lower near the cell membrane than the internal cytoplasm suggests that the environment is more crowded near the plasma membrane. The inner face of the cell membrane is a viscoelastic medium comprising actin filaments, which form a dense, cross-linked network with a mesh size of ~ 50 nm [28]. Within the actin cortex, a broad distribution of branching angles and different types of cross-linkages have been found [29]. The cortical actin filaments can also confine the particles in the mesh and act as barriers or obstacles for random walks. So in the cytosol, the particles have more space for movement than near the cellular surface because of less actin network. In other words, α_{1B}-AR is located or trapped in different networks.

4. Conclusion

This study demonstrated that real-time optical monitoring of the cellular trafficking of α_{1B}-ARs in living cells with high

spacial resolution is feasible, and this may provide a valuable tool for further study of the biochemical mechanism of ligand-induced receptor endocytosis. Trajectory analysis revealed the heterogeneous motion of α_{1B}-ARs–ligand complex in the cytosol of living cell, providing much more details than the fluorescence recovery after photobleaching and confocal laser scanning microscopy.

Acknowledgement

This work was supported by grants from the National Natural Science Foundation of China (20128003, 20333010, 30200342, 30490172) and NKBRSF (2006CB910304).

Appendix A. Supplementary data

Supplementary data associated with this article can be found, in the online version, at doi:10.1016/j.bpc.2007.01.009.

References

[1] J. Bockaert, J.P. Pin, Molecular tinkering of G protein-coupled receptors: an evolutionary success, EMBO J. 18 (1999) 1723–1729.
[2] G. Karp, Cell and Molecular Biology, Concepts and Experiments, John Wiley and Sons, Inc, 2005.
[3] L. Stanasila, J.B. Perez, H. Vogel, S. Cotecchia, Oligomerization of the alpha 1a- and alpha 1b-adrenergic receptor subtypes — potential implications in receptor internalization, J. Biol. Chem. 278 (2003) 40239–40251.
[4] M.A. Uberti, R.A. Hall, K.P. Minneman, Subtype-specific dimerization of alpha(1)-adrenoceptors: effects on receptor expression and pharmacological properties, Mol. Pharmacol. 64 (2003) 1379–1390.
[5] A. Vicentic, A. Robeva, G. Rogge, M. Uberti, K.P. Minneman, Biochemistry and pharmacology of epitope-tagged alpha(1)-adrenergic receptor subtypes, J. Pharmacol. Exp. Ther. 302 (2002) 58–65.
[6] T. Awaji, A. Hirasawa, M. Kataoka, H. Shinoura, Y. Nakayama, T. Sugawara, S. Izumi, G. Tsujimoto, Real-time optical monitoring of ligand-mediated internalization of alpha(1b)-adrenoceptor with green fluorescent protein, Mol. Endocrinol. 12 (1998) 1099–1111.
[7] D. Chalothorn, D.F. McCune, S.E. Edelmann, M.L. Garcia-Cazarin, G. Tsujimoto, M.T. Piascik, Differences in the cellular localization and agonist-mediated internalization properties of the alpha(1)-adrenoceptor subtypes, Mol. Pharmacol. 61 (2002) 1008–1016.
[8] M.I. Fonseca, D.C. Button, R.D. Brown, Agonist regulation of alpha(1b)-adrenergic receptor subcellular-distribution and function, J. Biol. Chem. 270 (1995) 8902–8909.
[9] A. Hirasawa, T. Sugawara, T. Awaji, K. Tsumaya, H. Ito, G. Tsujimoto, Subtype-specific differences in subcellular localization of alpha(1)-adrenoceptors: chlorethylclonidine preferentially alkylates the accessible cell surface alpha(1)-adrenoceptors irrespective of the subtype, Mol. Pharmacol. 52 (1997) 764–770.
[10] Y.Y. Zhang, K.M. Xu, C.D. Han, Alpha(1)-adrenoceptor subtypes mediating inotropic responses in rat heart, J. Pharmacol. Exp. Ther. 291 (1999) 829–836.
[11] T. Sugawara, A. Hirasawa, K. Hashimoto, G. Tsujimoto, Differences in the subcellular localization of alpha(1)-adrenoceptor subtypes can affect the subtype selectivity of drugs in a study with the fluorescent ligand BODIPY FL-prazosin, Life Sci. 70 (2002) 2113–2124.
[12] C. Hague, M.A. Uberti, Z.J. Chen, R.A. Hall, K.P. Minneman, Cell surface expression of alpha(1D)-adrenergic receptors is controlled by heterodimerization with alpha(1B)-adrenergic receptors, J. Biol. Chem. 279 (2004) 15541–15549.
[13] L.S. Barak, S.S.G. Ferguson, J. Zhang, C. Martenson, T. Meyer, M.G. Caron, Internal trafficking and surface mobility of a functionally intact beta (2)-adrenergic receptor-green fluorescent protein conjugate, Mol. Pharmacol. 51 (1997) 177–184.
[14] A.J. McLean, G. Milligan, Ligand regulation of green fluorescent protein-tagged forms of the human beta(1)- and beta(2)-adrenoceptors; comparisons with the unmodified receptors, Br. J. Pharmacol. 130 (2000) 1825–1832.
[15] M. Sunaguchi, M. Nishi, T. Mizobe, M. Kawata, Real-time imaging of green fluorescent protein-tagged beta(2)-adrenergic receptor distribution in living cells, Brain Res. 984 (2003) 21–32.
[16] M.J. Saxton, K. Jacobson, Single-particle tracking: applications to membrane dynamics, Ann. Rev. Biophys. Biomol. Struct. 26 (1997) 373–399.
[17] Y.H. Guan, Z. Wang, A.N. Cao, L.H. Lai, X.S. Zhao, Subunit exchange of MjHsp16.5 studied by single-molecule imaging and fluorescence resonance energy transfer, J. Am. Chem. Soc. 128 (2006) 7203–7208.
[18] M. Lakadamyali, M.J. Rust, H.P. Babcock, X. Zhuang, Visualizing infection of individual influenza viruses, PNAS 100 (2003) 9280–9285.
[19] G. Seisenberger, M.U. Ried, T. Endress, H. Buning, M. Hallek, C. Brauchle, Real-time single-molecule imaging of the infection pathway of an adeno-associated virus, Science 294 (2001) 1929–1932.
[20] A. Yildiz, J.N. Forkey, S.A. McKinney, T. Ha, Y.E. Goldman, P.R. Selvin, Myosin V walks hand-over-hand: single fluorophore imaging with 1.5-nm localization, Science 300 (2003) 2061–2065.
[21] A. Yildiz, M. Tomishige, R.D. Vale, P.R. Selvin, Kinesin walks hand-over-hand, Science 303 (2004) 676–678.
[22] C.J. Daly, C.M. Milligan, G. Milligan, J.F. Mackenzie, J.C. McGrath, Cellular localization and pharmacological characterization of functioning alpha-1 adrenoceptors by fluorescent ligand binding and image analysis reveals identical binding properties of clustered and diffuse populations of receptors, J. Pharmacol. Exp. Ther. 286 (1998) 984–990.
[23] R.E. Thompson, D.R. Larson, W.W. Webb, Precise nanometer localization analysis for individual fluorescent probes, Biophys. J. 82 (2002) 2775–2783.
[24] J.F. Mackenzie, C.J. Daly, J.D. Pediani, J.C. McGrath, Quantitative imaging in live human cells reveals intracellular alpha(1)-adrenoceptor ligand-binding sites, J. Pharmacol. Exp. Ther. 294 (2000) 434–443.
[25] J.C. McGrath, J.F. Mackenzie, C.J. Daly, Pharmacological implications of cellular localization of alpha(1)-adrenoceptors in native smooth muscle cells, J. Auton. Pharmacol. 19 (1999) 303–310.
[26] R.D. Vale, The molecular motor toolbox for intracellular transport, Cell 112 (2003) 467–480.
[27] J. Howard, Molecular motors: structural adaptations to cellular functions, Nature 389 (1997) 561–567.
[28] S.E. Sund, D. Axelrod, Actin dynamics at the living cell submembrane imaged by total internal reflection fluorescence photobleaching, Biophys. J. 79 (2000) 1655–1669.
[29] O. Medalia, I. Weber, A.S. Frangakis, D. Nicastro, G. Gerisch, W. Baumeister, Macromolecular architecture in eukaryotic cells visualized by cryoelectron tomography, Science 298 (2002) 1209–1213.